

## APPLIED SCIENCES AND ENGINEERING

## Vapor-printed polymer electrodes for long-term, on-demand health monitoring

Jae Joon Kim, Linden K. Allison, Trisha L. Andrew\*

We vapor print conformal conjugated polymer electrodes directly onto living plants and use these electrodes to probe the health of actively growing specimens using bioimpedance spectroscopy. Vapor-printed polymer electrodes, unlike their adhesive thin-film counterparts, do not delaminate from microtextured living surfaces as the organism matures and do not observably attenuate the natural growth pattern and self-sustenance of the plants investigated here. On-demand, noninvasive bioimpedance spectroscopy performed with long-lasting vapor-printed polymer electrodes can reliably detect deep tissue damage caused by dehydration and ultraviolet A exposure throughout the life cycle of a plant.

## INTRODUCTION

Emergent wearable health-monitoring devices use a tissue-adhered electrode as their sensing element, which is typically created by applying a preformed polymer, nanoparticle/nanowire, or carbon material film onto the outer surface of an organism (1). However, the surfaces of organisms display staggeringly diverse microscale features, and the complex biochemical, mechanical, and transport phenomena that operate at the interface between such microstructured living tissue and a man-made device ultimately control the performance and longevity of tissue-adhered electrodes (2). Contemporary stick-and-play devices, such as smart patches (3) and press-on buttons (4), are often susceptible to device delamination (5) from the surface of living organisms and often perturb air/water/nutrient transport at the biointerface, reducing long-term viability (6).

Here, we demonstrate a new paradigm for vapor printing biocompatible polymer films directly onto a living organism, creating conformal and long-lasting electrodes that allow long-term health monitoring using bioimpedance measurements. In this proof-of-concept study, we use live plants as a test bed, as they are abundant, have varied surface topographies, and are commonly used as biological models for many targeted biochemical studies (7, 8). Further, long-term plant health monitoring will also find strategic use in food farming, crop management, and biohazard signaling.

## RESULTS

Vapor printing affords robust and conformal polymer films on numerous topologically complex substrates (9, 10). We posited that this mild and remarkably versatile processing method could be further developed to create conducting polymer electrodes on living organisms, which could then be used to perform bioimpedance spectroscopy for health monitoring. Using a custom-built quartz wall reactor (11, 12), we printed functional polymer films directly on the surfaces of live seedlings, following the process outlined in Fig. 1A. A conducting polymer film was targeted for this pilot study so that long-lasting electrode pads could be created on the outer surfaces of plants. In particular, films of persistently *p*-doped poly(3,4-propylenedioxythiophene) (PProDOT-Cl; Fig. 1B) were explored because the particularly porous morphology (13, 14) of this mixed ion- and hole-conducting polymer is known to

enhance measurement accuracy during electronic impedance spectroscopy (15, 16). Entire plants, selectively masked samples, or severed plant parts were placed into the reactor, a mild vacuum (1000 mtorr) was applied, and monomer/oxidant vapors were introduced into the chamber to effect a vapor-phase polymerization that lead to polymer film growth on any exposed surface. All samples were held at room temperature during the entire vapor deposition operation, which lasted 20 min, on average. The coated samples thus obtained were rinsed with a dilute acid solution (0.1 mM HCl, 5 min) and distilled water to remove residual metal salts.

A selection of intact plants, cuttings, and leaves with diverse surface features was vapor-coated with PProDOT-Cl (Fig. 1 and fig. S1, A to I). Persistently, *p*-doped PProDOT-Cl is deep blue in color, and therefore, the presence of a conducting polymer coating could be visually identified and pristine samples could be easily distinguished from PProDOT-Cl-coated plant matter. Figure 1 shows pictures of various coated samples, including an intact air plant and a stonecrop cutting coated with a PProDOT-Cl electrode pattern. Energy-dispersive x-ray (EDX) spectroscopy of the surface of a coated palm leaf confirmed a uniform distribution of sulfur and chlorine atoms on the sample surface (fig. S2), consistent with the persistently doped polymer structure shown in Fig. 1B. Regardless of the size, scale, or density of the surface structures, uniform polymer coatings were successfully created on all exposed plant surfaces, without concomitant shriveling, cracking, bending, bleaching, or obvious chemical degradation of the samples (see magnified optical microscope images in fig. S1).

The detailed surface morphologies of pristine and PProDOT-Cl-coated plant leaves were imaged using scanning electron microscopy (fig. S3), which revealed that the intricate and varied surface microstructures of the leaves investigated here (ranging from simple, two-dimensional planar venations to three-dimensional, hierarchical, hairy structures) were continuously and conformally coated with PProDOT-Cl. The surface morphologies of all PProDOT-Cl coatings investigated here (the thickest coating was 5  $\mu\text{m}$ ) were faultless likenesses of the underlying plant surfaces, and scanning electron microscopy images of thick coatings did not reveal any polymer agglomeration or obvious sample corrosion (fig. S3, J and K). The hairy surfaces of geranium leaves, which can be considered model substrates for studying delamination of skin-adhered electronics (17), were also conformally coated with PProDOT-Cl. Notably, the vapor-deposited polymer coating did not fill or block the pores (stomata) of any leaf specimen, as shown in Fig. 1 (G and H) for pothos and aloe leaves, indicating that normal mass transport processes through these stomata could be maintained after coating.

Departments of Chemistry and Chemical Engineering, University of Massachusetts Amherst, Amherst, MA 01003, USA.

\*Corresponding author. Email: tandrew@umass.edu

Copyright © 2019  
The Authors, some  
rights reserved;  
exclusive licensee  
American Association  
for the Advancement  
of Science. No claim to  
original U.S. Government  
Works. Distributed  
under a Creative  
Commons Attribution  
NonCommercial  
License 4.0 (CC BY-NC).

Downloaded from <http://advances.sciencemag.org/> on March 18, 2019

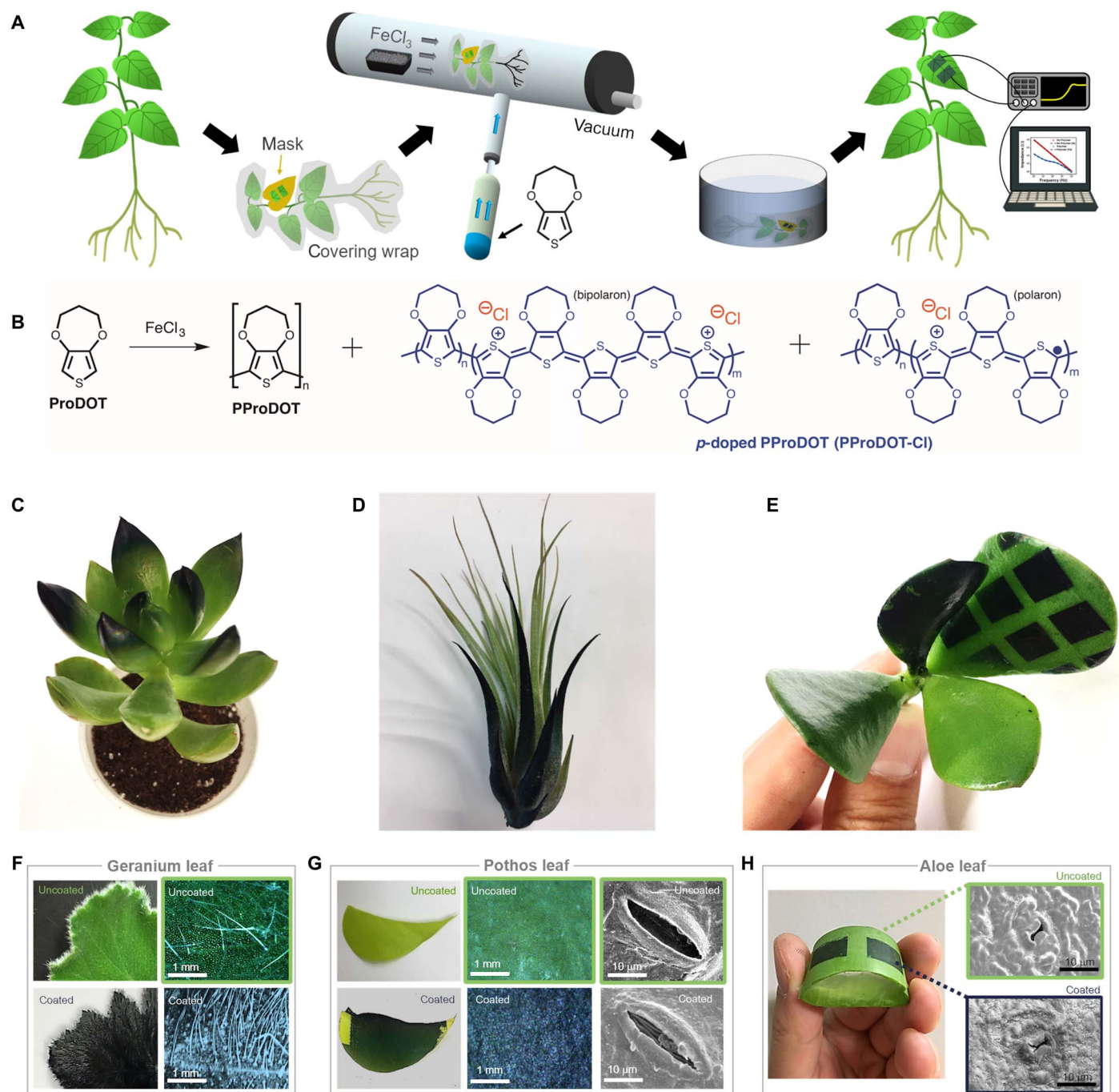


**Fig. 1. Vapor printing polymer films on plant matter.** (A) Process for vapor coating live plants with functional polymer films. (B) Oxidative polymerization reaction that occurs in the low-pressure reactor and structure of the conducting polymer coating, PProDOT-Cl, used in this work. (C) Stonecrop with the tips of selected leaves coated with PProDOT-Cl. (D) Air plant with the exposed surfaces of the outermost leaves coated with PProDOT-Cl. (E) Jade plant cutting coated with a PProDOT-Cl electrode pattern achieved using a polyimide tape mask placed on one leaf. (F) Digital photographs (left) and optical micrographs (right) of pristine and PProDOT-Cl-coated geranium leaves. (G) Digital photographs (left) and optical micrographs (center) of pristine and PProDOT-Cl-coated pothos leaves and scanning electron micrographs (SEMs; right) of a pristine and polymer-coated pothos stoma. (H) A digital photograph (left) of a cut aloe leaf vapor-coated with a PProDOT-Cl electrode pattern and SEMs (right) of a pristine and polymer-coated aloe stoma. Note that the gel inside a cut aloe leaf is preserved after vapor coating.

We quantified the water loss experienced by selected cut leaves upon being exposed to a 100-mtorr vacuum in our reactor for 20 min, which simulated the most severe of the vapor coating conditions used in this study. Water loss from plant matter can depend on the cell membrane structure and metabolism (18) of the sample and can be a barometer of

biological damage (19). Table S1 tabulates the relative water content of pristine plant matter and those of samples exposed to vacuum. The starting water content of the leaves investigated here was minimally altered upon exposure to vacuum, with only 5 to 7% water loss in palm, banana, bamboo, and geranium leaves and less than 2% water loss in

camellia, pine, pothos, and aloe leaves. These results confirmed that cut leaf samples, which are especially susceptible to evaporative water loss through exposed pores as compared to intact plants, suffered negligible dehydration during the vapor coating operation, in accordance with the pictures shown in Fig. 1H. Notably, the gel inside the aloe leaf was preserved, with its viscosity unchanged after being subjected to vapor coating.

To prove that the vapor coating operation and/or the PProDOT-Cl coating itself did not perturb the natural biological functions of plant matter, we first explored the longevity of severed, non-self-sustaining plant organs—namely flowers—to establish the effects of the surface coating in the absence of external nutrition and photosynthesis. Freshly plucked hoyia flowers were vapor-coated with a 500-nm-thick PProDOT-Cl film, rinsed, and placed into a vase with water, and their longevity was compared to those of pristine flowers plucked from the same cluster of the same plant (Fig. 2A, Movie Hoya Flower); these experiments were repeated on three such sets of flowers. Both pristine and polymer-coated hoyia flowers showed comparable stabilities during the first day of monitoring. Moreover, both samples, on average, displayed approximately similar decay rates over 80 hours of monitoring. This observation suggested that coated hoyia flowers were able to uptake air, water, and/or nutrients and maintain vitality to the same degree as an uncoated control sample.

Next, we deposited a patterned polymer electrode array on pothos and stoncrop seedlings and investigated their growth characteristics (Fig. 2B). Small-sized seedlings were selected to accommodate the radius (10 cm) of our laboratory-scale reactor. The process of vapor coating a stoncrop seedling is depicted in fig. S4 (A to F). The root system of the seedlings remained enclosed in damp soil within a plastic bag to limit dehydration and chemical stress during vapor coating. Major parts of the seedling were also masked with either a cutout plastic sheetmask or a tape mask to delineate the desired electrode pattern on specific leaves. The PProDOT-Cl-coated leaf of the pothos seedling appeared to droop immediately after vapor coating (Fig. 2B). However, after 15 days of indoor growth in water and under moderate sunlight, the seedling displayed clear signs of health and vitality. First, intensive root growth was evident. The erstwhile-drooping, PProDOT-Cl-coated leaf became visibly greener in color (indicating chlorophyll production; table S2) and gradually grew to face upward, toward the sunlight. Further, the seedling continued to grow after transplanting into potting soil, and two new leaves appeared 45 days after the vapor coating operation. On the basis of these three observations, i.e., new root and leaf growth (20), phototropism (21), and an increase in chlorophyll content (22), we concluded that the pothos seedling remained healthy, self-sustaining, and reproductive after vapor coating. Similar root/leaf growth, phototropism, and chlorophyll production were also observed in two other separately coated pothos seedlings (fig. S4, G and H), supporting the claim that our vapor coating operation did not harm plant health.

The PProDOT-Cl surface coatings displayed, on average, electronic conductivities of 1 S/cm (Fig. 2C), which is sufficient enough for these films to serve as conductive electrodes for bioimpedance spectroscopy. Higher conductivities, up to 200 S/cm, could be achieved if plant matter were heated to 60°C during vapor coating, but these conditions damaged live specimens. The PProDOT-Cl coating on either monocotyledonous or dicotyledonous leaves did not display directional anisotropy in conductivity, likely because any organizational order imposed in the polymer coating by these leaf venations occurs at much longer length scales (in micrometers) than the characteristic  $\pi$ -stacking length scale (0.4 to 10 nm) that influences electronic conductivity in

conjugated polymers. The conductivity of PProDOT-Cl (1  $\mu$ m) vapor-deposited on untreated glass was measured to be 1.21 S/cm, further confirming the absence of substantial substrate effects on charge transport properties. The surface roughness of a 1- $\mu$ m-thick film of PProDOT-Cl on glass was measured to be 33.9 nm using atomic force microscopy, and its water contact angle was 60°. The PProDOT-Cl coatings on plant leaves displayed remarkable surface adhesion and mechanical robustness, similar to previous reports on vapor-printed films (9, 10, 12). The PProDOT-Cl coating on a palm leaf did not crack or delaminate when the palm leaf was strained or bent to an angle of nearly 90° (Fig. 2D and fig. S1J). Further, the observed resistance of the PProDOT-Cl coating only fluctuated by approximately  $\pm 5\%$  over multiple bend/release cycles. To contextualize these results, consider the mechanical robustness of a solution cast conducting polymer coating created on a palm leaf: A one-time application of 1% strain immediately caused multiple centimeter-sized cracks and film delamination (fig. S1K). The electrical properties of the PProDOT-Cl coatings also remained invariant upon exposure to water or humid environments (Fig. 2E), meaning that coated plants could be grown in their preferred native environments without fear of damaging the polymer electrodes.

Encouraged by the observed ruggedness, stable conductivity, and minimal invasiveness of our vapor-printed PProDOT-Cl coatings, we progressed to investigating their use in long-term plant health monitoring. Bioimpedance spectroscopy is a sensitive analytical technique capable of quantifying cellular water content and revealing details about cell wall composition. This information can be used to diagnose many biotic and abiotic stress factors in plants (23, 24), particularly drought stress. However, accurate impedance measurements on plants typically necessitate the use of metal needles to pierce plant tissue and create viable electrical contact [with a few developing exceptions (8, 25)], which irreparably damages the test site and may lead to plant death (26). Therefore, despite the wealth of information that can be potentially gleaned from a single impedance spectroscopy measurement, this method is not widely used by plant biologists. We hypothesized that our robust, noninvasive PProDOT-Cl coatings could be used as conductive contact pads with which to perform bioimpedance spectroscopy for on-demand plant health monitoring.

For this pilot study, we chose to focus on PProDOT-Cl-coated leaves as potential electrodes for bioimpedance spectroscopy, instead of plant stems, flowers, or roots, because leaves can be easily vapor-coated with a polymer pattern (Fig. 3A). Mature or nearly mature leaves were chosen for this work to avoid aging-related changes specific to a single leaf and to establish a bioimpedance baseline for the overall health of a growing plant. Further, only one leaf per seedling was coated with a PProDOT-Cl electrode pattern for experimental simplicity and also for understanding variations in bioimpedance signals recorded from the same leaf of the same plant over a long period of growth. Figure 3 (B and C) shows the frequency-dependent impedance and phase responses, respectively, recorded from one PProDOT-Cl-coated leaf of a pothos seedling, measured immediately after vapor coating and after 45, 90, and 130 days of growth in water and soil. In the diagnostically important region above  $10^3$  Hz, both impedance and phase responses varied by only 3% over 130 days as the seedling matured, as expected for a disease-free, undamaged, actively growing plant. Significant differences were only observed in the comparatively unimportant, low-frequency ( $<10^3$  Hz) range over 130 days of monitoring, which can be ascribed to variations in electrode contact resistance that likely arise because the leaf epidermis changes as the seedling grows (e.g., the leaf surface becomes thicker and waxier). This result confirmed that the

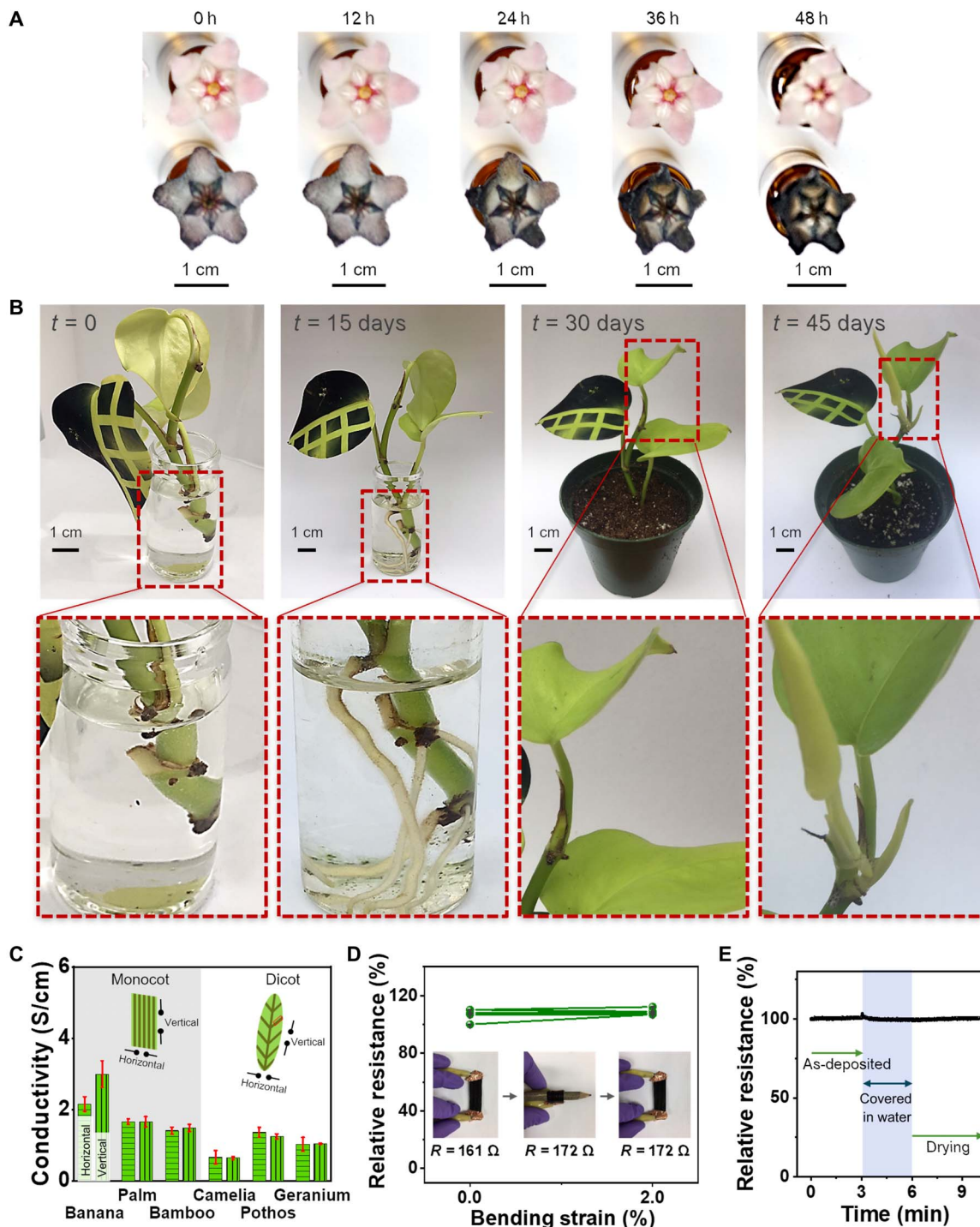


**Fig. 2. Health of vapor-coated plant matter.** (A) Pictures of pristine (top) and polymer-coated (bottom) hoya flowers monitored over 48 hours. The flowers were kept in a vial filled with tap water. Note that the observed (reflected) color of the polymer coating varies depending on the underlying structure of the flower petal. The polymer coating is uniformly 500 nm thick on the plant surface. (B) Undoctored digital photographs of a PProDOT-Cl-coated pothos seedling immediately after vapor coating ( $t = 0$ ), after 15 days of growth in water ( $t = 15$  days), 15 days after transplanting the seedling into potting soil ( $t = 30$  days), and 30 days after growth in potting soil ( $t = 45$  days). Note the phototropism and increased chlorophyll content in the PProDOT-Cl-coated leaf. New roots and leaves are highlighted in the second row of photographs. (C) Surface conductivities of the PProDOT-Cl coating on selected monocotyledonous and dicotyledonous leaves measured in two different directions, as explained by the cartoon inset. Resistance change of a 1- $\mu$ m-thick PProDOT-Cl coating on a palm leaf monitored (D) over repeated bending cycles and (E) upon wetting the leaf with water and allowing passive evaporation. The insets in (D) are pictures of the palm leaves during the bending tests.

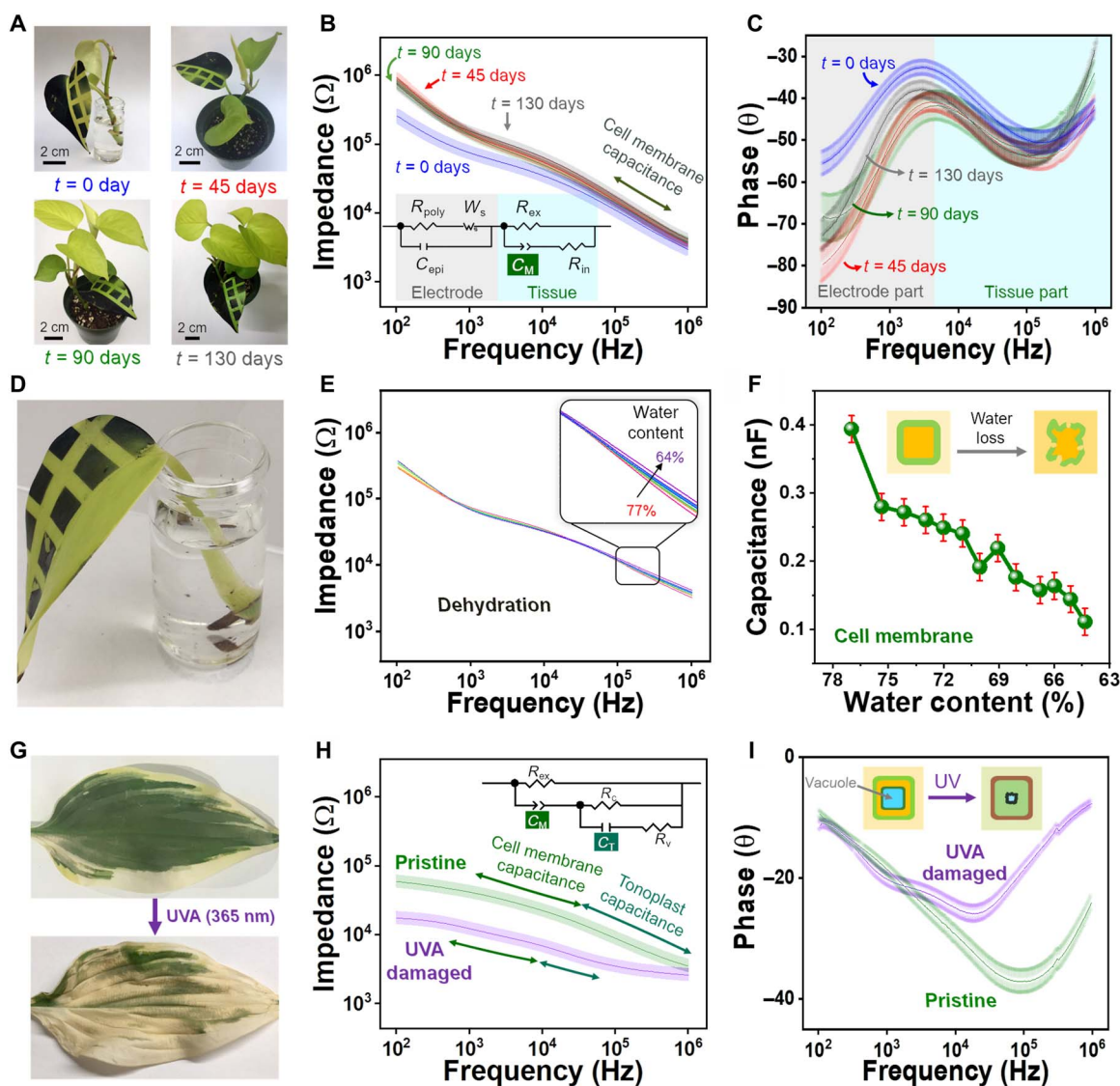


**Fig. 3. Bioimpedance spectroscopy on live plants coated with PProDOT-Cl electrode pads.** (A) Pictures of a polymer-coated pothos seedling over a 130-day monitoring period. Frequency-dependent (B) impedance and (C) phase response of the pothos seedling measured immediately after vapor coating and after 45, 90, and 130 days of growth in water and soil. The shaded regions indicate the variation of the measured data. The inset in (B) depicts the circuit model used to interpret the impedance measurements. (D) Picture of a polymer-coated pothos leaf used to detect drought stress. (E) Frequency-dependent impedance response of the same pothos leaf at various stages of dehydration. (F) Cell membrane capacitance ( $C_M$ ) as a function of the water content of a pothos leaf. The inset cartoon depicts cell membrane changes caused by drought stress. Cell membrane capacitances were extracted using the circuit model shown as an inset in (B). (G) Pictures of a pristine and UVA-irradiated hosta leaf. The fluence of UVA irradiation is equivalent to 9.5 days of sunlight. Frequency-dependent (H) impedance and (I) phase response of a pristine (green) and UVA-exposed (purple) hosta leaf. The inset in (H) shows the equivalent circuit model used to quantify tissue health. The cartoon inset in (I) summarizes cell damage caused by UVA exposure.

vapor-coated PProDOT-Cl coatings can serve as robust electrodes for long-term, on-demand plant health monitoring.

The inset in Fig. 3B shows the equivalent circuit used to model and interpret the bioimpedance measurements of the growing pothos seedling. Two components comprise the equivalent circuit: an electrode component that arises due to the internal resistance of the PProDOT-Cl coating ( $R_{poly}$ ), the capacitance of the leaf epidermis ( $C_{epi}$ ), and ion transport/voltage drop across the polymer/epidermis interface ( $W_s$ ) and a tissue component that reflects the health of the sample. The electrode component is dominant at low frequencies ( $<10^3$  Hz), and the tissue component is dominant at high frequencies ( $>10^3$  Hz). De-

pending on the specific plant sample and growth/stress conditions, multiple subparts can be invoked for the tissue circuit component, including cell membrane capacitance ( $C_M$ ), extracellular fluid resistance ( $R_{ex}$ ), intracellular fluid resistance ( $R_{in}$ ), tonoplast capacitance ( $C_T$ ), vacuole fluid resistance ( $R_v$ ), and cytoplasm fluid resistance ( $R_c$ ). We used a simple circuit model to understand the tissue components of the growing pothos seedling, including only three components:  $C_M$ ,  $R_{ex}$ , and  $R_{in}$ . Table S3 lists the extracted values for these three tissue components obtained from impedance measurements taken on a pothos seedling over 130 days of active growth; the low  $\chi^2$  values for all extracted components confirm the accuracy of our equivalent circuit model.

Next, we sought to prove that bioimpedance measurements performed using PProDOT-Cl electrode pads on a leaf could reliably detect drought stress in leaf tissue. We used severed pothos leaves for this exercise so that we could controllably decrease water content in a sample by applying vacuum and because pothos leaves were observed to remain especially hardy upon being dehydrated. To artificially simulate varying degrees of drought stress, test leaves were dried in a vacuum oven (0.5 mtorr) held at room temperature, and their mass change and impedance response were measured every 10 min. The decrease in water content of the leaf manifested as a gradual change in the tissue-derived sections ( $>10^4$  Hz) of the recorded impedance (Fig. 3E) and phase (fig. S5A) responses. Using the same circuit model described above, we extracted values for  $R_{in}$ ,  $C_M$ , and  $R_{ex}$ . Both  $R_{ex}$  and  $C_M$  linearly decreased with decreasing water content in pothos leaves, whereas  $R_{in}$  remained mostly constant (fig. S5B). Notably, a 13% decrease in leaf water content (from 77 to 64%) resulted in a 70% decrease in the observed cell membrane capacitance and a 30% decrease in the extracellular fluid resistance. These can be explained by a breakdown of cell membranes and accompanying leakage of ion-rich intracellular fluid, which will lower the cell membrane capacitance and increase the conductivity of the extracellular fluid (27). This observed high precision qualifies our method as superior to existing spectroscopic methods to remotely detect drought stress, which typically require  $>52\%$  water loss to produce a viable signal (28). The  $C_M$  values extracted from a healthy leaf of an adequately hydrated pothos seedling varied by only 3% over 130 days of active growth (table S3), meaning that significant changes in cell membrane capacitance can be reliably ascribed to drought stress.

Further, we demonstrated that bioimpedance spectroscopy performed using PProDOT-Cl contact pads could reveal deep tissue damage in plant leaves caused by ultraviolet A (UVA) irradiation. We focused on UVA (320 to 400 nm) radiation, specifically because it is known to penetrate deeper into living tissue as compared to UVB and UVC radiation and cause damage that can often go undetected by conventional, on-surface detection systems (29, 30).

We used the leaves of a hosta plant for this study, as the leaves of this shade-loving perennial are especially susceptible to photo-damage. The frequency-dependent impedance and phase responses of a hosta leaf (Fig. 3, H and I) did not show an appreciable signal arising from electrode contact and were mostly dominated by two capacitive tissue components:  $C_M$  and  $C_T$ . This pattern is different from the impedance response observed for pothos leaves, likely because of structural differences between pothos and hosta leaves: Hosta leaves have a thinner epidermis (meaning that the effect of electrode contact resistance is decreased) and an additional tonoplast that divides the intracellular contribution into a vacuole and cytoplasm (31). The equivalent circuit used to model the bioimpedance response of hosta leaves is depicted in the inset of Fig. 3H, and numerical values for the tissue components extracted from this model are tabulated in table S4.

A picture and explanation of our UVA irradiation setup are provided in fig. S6. Attention was paid to keep the hosta leaf hydrated during UVA exposure and to filter out infrared light emitted from our light source so that sample dehydration due to photon heating would be minimized. After 4 hours of continuous exposure to UVA irradiation ( $16.01 \text{ mW/cm}^2$ ), which is equivalent to 9.5 days of daylight exposure, a healthy, variegated hosta leaf turned pale yellow because of a decrease in chlorophyll content (Fig. 3G). Accordingly, the frequency-dependent impedance and phase responses of the UVA-irradiated hosta leaf changed drastically. The resistance of the vacuole fluid ( $R_v$ )

increased by 170% upon UVA exposure, whereas the resistances of the extracellular and cytoplasm fluids decreased by 70 and 50%, respectively. These trends can be ascribed to the leakage of intracellular vacuole fluid into the extracellular matrix due to photodamage (32). Values for both  $C_M$  and  $C_T$  increased by 370 and 80%, respectively, upon UVA irradiation because of the polarization of these membrane components by UV-induced radicals (33). The bioimpedance measurement could distinguish damage caused by UVA irradiation from cell membrane damage caused by drought stress (dehydration), which typically results in a decrease in the membrane capacitance values.

## DISCUSSION

We vapor-printed conformal and durable conducting polymer electrodes directly onto living plants and used these electrodes to probe the health of actively growing plant specimens using bioimpedance spectroscopy. The vapor-printed electrodes do not observably influence the natural growth pattern and self-sustenance of the investigated plant specimens and can be used as long-lasting diagnostic handles for detecting stressors, such as drought and photodamage, in plants. This work established the groundwork for sensitively performing on-demand health tests throughout the life cycle of a plant, which will find strategic use in food farming, crop management, and biohazard signaling.

## MATERIALS AND METHODS

### Chemicals and plant specimens

All plant specimens were collected from Durfee Conservatory at the University of Massachusetts Amherst. Plants used in this study were stonecrop (*Sedum nussbaumerianum*), air plant (*Tillandsia stricta*), jade plant (*Crassula argentea*), pothos (*Epipremnum aureum*), banana (*Musa acuminata*), bamboo (*Phyllostachys aurea*), pine (western yellow pine, *Pinus ponderosa*), geranium (peppermint-scented geranium, *Pelargonium tomentosum*), palm (Texana Sabal palm, *Sabal mexicana*), camellia (*Camellia japonica*), aloe (*Aloe vera*), lemongrass (*Cymbopogon citriodora*), hoyo (*Hoya carnosa*), and hosta (*Hosta pilgrim*). Leaves were picked from a living plant directly, rinsed with distilled water, and introduced into our vapor deposition chamber without any surface treatment. The monomer 3,4-propylenedioxythiophene (ProDOT), oxidant iron chloride ( $\text{FeCl}_3$ ), and solution-processed composite material, poly(3,4-ethylenedioxythiophene)-poly(styrene sulfonate) (PEDOT:PSS) (0.5 to 1 weight % in water), were purchased from Sigma-Aldrich and used without any purification.

### Vapor coating

A custom-built, quartz, hot wall reactor was used to polymerize ProDOT (monomer) directly on the surface of live plants. The pressure of the reactor was maintained at 1000 mtorr during the entire deposition process. The reactor was heated using temperature-controlled fiberglass heating tape (BIH101060L, BriskHeat) wrapped around the central quartz tube. Two thermocouples were attached on the outer glass wall of the central tube and monomer ampule, where oxidant and monomer were placed. The solid oxidant  $\text{FeCl}_3$  was placed inside a ceramic boat and sublimed at  $200^\circ\text{C}$ . For vapor coating of living and hydrated plant matter, only the part of the central quartz tube containing the oxidant crucible was heated. To prevent thermal damage, plant matter were placed at least 15 cm away from the oxidant crucible such that the plant samples remained at room temperature. The ampule containing the monomer ProDOT was heated to  $80^\circ\text{C}$ .

After the oxidant crucible was heated and an oxidant halo was observed to form in the central tube, monomer vapors were introduced into the central tube by opening a needle valve. Oxidative polymerization proceeded in the middle of the tube where monomer and oxidant vapors met. Polymer formation could be recognized by the evolution of a royal blue color. Polymer coating thickness was controlled by varying the deposition time (shorter time, thin film; longer time, thick film). A previously developed calibration curve of time-dependent film thickness (11, 12) was used as a guide. For this work, polymer growth was allowed to proceed for 20 min, on average, resulting in uniform, 1- $\mu\text{m}$ -thick coatings on plant specimens. Although it was previously demonstrated that Fe(III) salts were nontoxic to plant matter (fruits) (34), residual oxidant and monomer were removed from the PProDOT-Cl-coated samples by dipping the plant matter into a dilute acid solution (0.1 mM) for 5 min and subsequently distilled water for 5 min. Extra moisture on the surface was wiped off with Texwipes. To create spatially patterned electrodes, polyimide tape was placed directly on the sample surface before deposition and was lifted off immediately after the deposition.

### Relative water content

The relative water content (RWC) of each leaf was calculated using Eq. 1

$$\text{RWC}(\%) = \frac{\text{Fresh weight} - \text{Dry weight}}{\text{Turgid weight} - \text{Dry weight}} \times 100(\%) \quad (1)$$

The dry weight was determined by heating each sample at 70°C for >5 days until the measured mass did not change. The turgid weight was measured after immersing fresh leaves in distilled water for 5 hours in the dark and removing extra water on the surface with Texwipes.

### Plant health and liveliness testing

The petals of hoyia flowers were coated with an approximately 500-nm-thick film of PProDOT-Cl, leaving the stems and the cut stem edges uncoated. The cut stem ends were immediately placed in a vial of unfiltered tap water immediately after vapor coating and rinsing. Stonecrop, air plant, jade plant, and pothos seedlings were selected for their small sizes. For long-term observation, the stems of pristine and polymer-coated pothos seedlings were placed into a transparent, water-filled vial to enable real-time monitoring of root growth. Subsequently, the rooted seedlings were transplanted into potting soil for further growth. Growing seedlings (either in water or in soil) were placed inside a greenhouse at the Durfee Conservatory with sunlight consistently arriving from the ceiling to probe phototropism.

The chlorophyll content of the polymer-coated leaves was calculated from digital photographs using Eq. 2

$$\text{Chlorophyll content (g m}^{-2}\text{)} = 0.952 - 1.76 \times \frac{R - B}{R + B} \quad (2)$$

where  $R$  and  $B$  are the values of the red and blue channels, respectively, in the undoctored digital image. Using this equation, the change of chlorophyll content could be correlated to the color change of the undoctored digital image (35). The values of RGB were extracted using Adobe Photoshop on the same physical spot in each leaf photo shown in fig. S4G. This approximate photogrammetric approach to quantify-

ing leaf chlorophyll content was only performed for seedlings placed in water.

### UVA irradiation

UVA (365 nm) radiation was created using an OAI 500 W UVA source, and the fluence was measured with a UV power meter (OAI 306). A water-filled petri dish was placed in the path of light before the plant sample to filter short-wavelength UV light and infrared light. To prevent sample dehydration during irradiation, the cut edge of hosta leaves was packed with a water-soaked cotton ball. The daylight equivalence of the artificial UVA fluence generated by our light source was calculated to be 1.4 days per hour of irradiation, using a previously reported formula (36), and the standard daylight metrics for Chicago, United States (latitude 41.9°), and a UVA/UVB ratio of 23. Polymer electrodes were vapor-deposited onto the hosta leaves after UVA irradiation to accurately characterize the bioimpedance signal of a UVA-damaged hosta leaf while excluding errant signal changes arising from photodamage to the PProDOT-Cl coating.

### Morphology and electrical characterization

The thicknesses of PProDOT-Cl coatings were measured with an optical profilometer (Zygo NewView 7300, Veeco Dektak 150, and Veeco NT9080). The optical images and videos of the coated plant matter were captured with an optical microscope (Zeiss Axio Scope.A1 equipped with a Zeiss AxioCam IC1 camera) or a digital camera (K-30, Pentax). Atomic force microscopy (AFM) was performed using a Bruker MultiMode AFM. Water contact angles were measured using an Attension Theta contact angle meter. Scanning electron micrographs (SEMs) were captured using a Magellan 400 XHR SEM equipped with an Oxford X-MAX 80-mm<sup>2</sup> EDX spectrometer for element mapping. The surface conductivity of PProDOT-Cl on plant matter was measured using a four-probe measurement station (Pro4-440N, Lucas Labs) equipped with an SP4 probe head. The tip spacing was 1.27 mm, and the tip radius was 0.04 mm. The tip was made of tungsten carbide.

### Mechanical and water stability

The resistances of the PProDOT-Cl coatings were continuously measured with a Keithley 4200-SCS probe station under various environmental conditions. For the bending tests, PProDOT-Cl-coated palm leaves were wrapped around three-dimensional-printed cylinders of varying diameters to simulate strain. Alligator clips and copper tape were used to make stable electrical contacts to the polymer coating while bending. The water stability of the PProDOT-Cl electrode was characterized by comparing the resistance of the dry polymer on a palm leaf with that of the polymer after submerging the palm leaf into water and drying under ambient conditions. Adhesion tests were performed by applying 1% stain on each leaf with polymer electrodes prepared by either solution casting (PEDOT:PSS) or vapor coating (PProDOT-Cl). Commercial aqueous PEDOT:PSS was dropcast onto palm leaves and annealed at 120°C under ambient conditions for 1 hour before mechanical testing.

### Bioimpedance spectroscopy

Bioimpedance spectroscopy was performed with an Agilent 4294A precision impedance analyzer over a frequency range of 100 Hz to 1 MHz. The measurement was performed at low applied potential (100 mV) to prevent unwanted doping/dedoping reactions in the PProDOT-Cl coatings. The ZView2 software (Princeton Applied Research)

was used to fit the acquired data to an equivalent circuit and extract values for various circuit components.

Frequency-dependent impedance and phase responses were recorded using PProDOT-Cl contact pads immediately after deposition, rinsing, and drying. Polymer electrodes of 6.35-mm width and 3.18-mm inter-electrode spacing were created on each leaf surface using polyimide tape masking. We used silver metal probe tips mounted on a micro-manipulator to connect to our custom-built probe station. To make electrical contact between our instrument's probe tips and the PProDOT-Cl electrode, a droplet of 0.1 M aqueous NaCl was placed over each PProDOT-Cl electrode and the metal probe tip was lowered into this NaCl droplet. The NaCl droplet normalized the area of the polymer electrode, especially for long-term monitoring of growing seedling samples, and also eliminated contact resistance between the probe tip and the polymer electrode. Because all the leaves investigated here had hydrophobic surfaces but the PProDOT-Cl coating was hydrophilic, the NaCl droplet was automatically spatially confined to the area of the polymer electrode and did not wet the entire leaf surface. The NaCl droplet was rinsed off with distilled water after measurement. For drought monitoring, polymer-coated pothos leaves were placed in vacuum oven held at room temperature to effect dehydration and their impedance was recorded every 10 min. The leaves were cut in half along their long axis to accelerate dehydration. The decrease of relative water content was quantified by weighing the leaf at each time interval.

### Equivalent circuit models for bioimpedance spectroscopy

To ascertain information about electrical contact, cell membrane integrity, and fluid content, the recorded impedance data were fitted in ZView2 using equivalent circuit models containing an electrode and tissue components. The electrode component was composed of a resistor, a capacitor, and a transmissive Warburg component, following the modified Randles model (37). The resistor,  $R_{\text{poly}}$ , represented the intrinsic conductivity of the PProDOT-Cl coating. The capacitor,  $C_{\text{epi}}$ , accounted for the capacitance introduced by the insulating leaf epidermis. The transmissive Warburg component,  $W_s$ , accounted for ion diffusion between the polymer coating and leaf cells and was composed of three subparts: a diffusion impedance constant,  $A_W$ ; a Warburg exponent,  $p$ ; and a characteristic ion diffusion time,  $B_W$ . Additional circuit components for the NaCl droplet were not necessary to accurately fit the recorded data in the frequency range used in this study.

For the pothos tissue component, the Hayden model (38) was used to translate three principal cellular components of a pothos leaf into discrete circuit elements: Extracellular fluid was represented by a resistor,  $R_{\text{ex}}$ ; intracellular fluid was represented by a resistor,  $R_{\text{in}}$ ; and the cell membrane was represented by a capacitor,  $C_M$ . The cell membrane capacitance was represented in the circuit as a constant phase element ( $CPE_M$ ) instead of a simple capacitor because the tissue was composed of an ensemble of cells that result in electronic dispersity. The value for  $C_M$  was extracted from  $CPE_M$  using Eq. 3

$$C_M = Y_0^{\frac{1}{p}} (R_{\text{in}} + R_{\text{ex}})^{\frac{1-p}{p}} \quad (3)$$

where  $Y_0$  is the CPE constant and  $p$  is the CPE exponent.

For hosta leaves, which display a thin epidermis, the electrode part did not manifest in the recorded impedance data over the frequency range of our experiment. For the tissue part, an additional tonoplast capacitor ( $C_T$ ) was included in the circuit model and the intracellular components were divided into two components: cytoplasm fluid resistor ( $R_c$ ) and vacuole fluid resistor ( $R_v$ ). These extra components arise from the double shell model of leaf tissue (26, 31).

### SUPPLEMENTARY MATERIALS

Supplementary material for this article is available at <http://advances.sciencemag.org/cgi/content/full/5/3/eaaw0463/DC1>

Movie Hoya Flower. A comparison of the longevity of pristine and PProDOT-Cl-coated hoya flowers over 81 hours.

Fig. S1. Images of polymer-coated plant matter.

Fig. S2. EDX spectra of pristine and polymer-coated leaves.

Fig. S3. Imaging the surfaces of pristine and PProDOT-Cl-coated leaves.

Fig. S4. Polymer coating procedure and subsequent seedling growth.

Fig. S5. Impedance analysis of drought stress.

Fig. S6. UVA irradiation of hosta.

Table S1. Relative water content of plant matter.

Table S2. Optical estimation of chlorophyll content.

Table S3. Impedance components and long-term health monitoring.

Table S4. Impedance components for pristine and UV-irradiated hosta leaves.

### REFERENCES AND NOTES

1. D.-H. Kim, N. Lu, R. Ma, Y.-S. Kim, R.-H. Kim, S. Wang, J. Wu, S. M. Won, H. Tao, A. Islam, K. J. Yu, T. I. Kim, R. Chowdhury, M. Ying, L. Xu, M. Li, H. J. Chung, H. Keum, M. McCormick, P. Liu, Y.-W. Zhang, F. G. Omenetto, Y. Huang, T. Coleman, J. A. Rogers, Epidermal electronics. *Science* **333**, 838–843 (2011).
2. A. Miyamoto, S. Lee, N. F. Cooray, S. Lee, M. Mori, N. Matsuhisa, H. Jin, L. Yoda, T. Yokota, A. Itoh, M. Sekino, H. Kawasaki, T. Ebihara, M. Amagai, T. Someya, Inflammation-free, gas-permeable, lightweight, stretchable on-skin electronics with nanomeshes. *Nat. Nanotechnol.* **12**, 907–913 (2017).
3. W.-H. Yeo, Y.-S. Kim, J. Lee, A. Ameen, L. Shi, M. Li, S. Wang, R. Ma, S. H. Jin, Z. Kang, Y. Huang, J. A. Rogers, Multifunctional epidermal electronics printed directly onto the skin. *Adv. Mater.* **25**, 2773–2778 (2013).
4. J. Kim, P. Gutruf, A. M. Chiarelli, S. Y. Heo, K. Cho, Z. Xie, A. Banks, S. Han, K. I. Jang, J. W. Lee, K. T. Lee, X. Feng, Y. Huang, M. Fabiani, G. Gratton, U. Paik, J. A. Rogers, Miniaturized battery-free wireless systems for wearable pulse oximetry. *Adv. Funct. Mater.* **27**, 1604373 (2017).
5. H. Cheng, S. Wang, Mechanics of interfacial delamination in epidermal electronics systems. *J. Appl. Mech.* **81**, 044501 (2014).
6. S. K. Vashist, Non-invasive glucose monitoring technology in diabetes management: A review. *Anal. Chim. Acta* **750**, 16–27 (2012).
7. E. Stavrinidou, R. Gabrielsson, E. Gomez, X. Crispin, O. Nilsson, D. T. Simon, M. Berggren, Electronic plants. *Sci. Adv.* **1**, e1501136 (2015).
8. V. B. Koman, T. T. Lew, M. H. Wong, S.-Y. Kwak, J. P. Giraldo, M. S. Strano, Persistent drought monitoring using a microfluidic-printed electro-mechanical sensor of stomata in planta. *Lab Chip* **17**, 4015–4024 (2017).
9. A. M. Coclite, R. M. Howden, D. C. Borrelli, C. D. Petruczuk, R. Yang, J. L. Yagüe, A. Ugur, N. Chen, S. Lee, W. J. Jo, A. Liu, X. Wang, K. K. Gleason, 25th Anniversary article: CVD polymers: A new paradigm for surface modification and device fabrication. *Adv. Mater.* **25**, 5392–5423 (2013).
10. P. Moni, A. Al-Obeidi, K. K. Gleason, Vapor deposition routes to conformal polymer thin films. *Beilstein J. Nanotechnol.* **8**, 723–735 (2017).
11. N. Cheng, T. L. Andrew, Reactive vapor deposition of conjugated polymer films on arbitrary substrates. *J. Vis. Exp.* **131**, e56775 (2018).
12. N. Cheng, L. Zhang, J. J. Kim, T. L. Andrew, Vapor phase organic chemistry to deposit conjugated polymer films on arbitrary substrates. *J. Mater. Chem. C* **5**, 5787–5796 (2017).
13. P. M. Beaujuge, J. R. Reynolds, Color control in  $\pi$ -conjugated organic polymers for use in electrochromic devices. *Chem. Rev.* **110**, 268–320 (2010).
14. Y. Sulaiman, R. Katakly, Effect of monomer modifications on the physical properties of electropolymerised PEDOT films. *J. Electrochem. Soc.* **159**, F1–F9 (2011).
15. T. Pajkossy, Impedance spectroscopy at interfaces of metals and aqueous solutions—Surface roughness, CPE and related issues. *Solid State Ion.* **176**, 1997–2003 (2005).
16. R. A. Green, N. H. Lovell, G. G. Wallace, L. A. Poole-Warren, Conducting polymers for neural interfaces: Challenges in developing an effective long-term implant. *Biomaterials* **29**, 3393–3399 (2008).
17. K.-I. Jang, S. Y. Han, S. Xu, K. E. Mathewson, Y. Zhang, J.-W. Jeong, G.-T. Kim, R. C. Webb, J. W. Lee, T. J. Dawidczyk, R. H. Kim, Y. M. Song, W.-H. Yeo, S. Kim, H. Cheng, S. I. Rhee, J. Chung, B. Kim, H. U. Chung, D. Lee, Y. Yang, M. Cho, J. G. Gaspar, R. Carbonari, M. Fabiani, G. Gratton, Y. Huang, J. A. Rogers, Rugged and breathable forms of stretchable

- electronics with adherent composite substrates for transcutaneous monitoring. *Nat. Commun.* **5**, 4779 (2014).
18. J. S. Boyer, Advances in drought tolerance in plants. *Adv. Agron.* **56**, 187–219 (1996).
  19. E. A. Bray, Plant responses to water deficit. *Trends Plant Sci.* **2**, 48–54 (1997).
  20. A. Hodge, G. Berta, C. Doussan, F. Merchan, M. Crespi, Plant root growth, architecture and function. *Plant Soil* **321**, 153–187 (2009).
  21. J. Friml, Auxin transport—Shaping the plant. *Curr. Opin. Plant Biol.* **6**, 7–12 (2003).
  22. J. P. Palta, Leaf chlorophyll content. *Remote Sens. Rev.* **5**, 207–213 (1990).
  23. A. Y. Khaled, S. Abd Aziz, S. K. Bejo, N. M. Nawwi, I. A. Seman, D. I. Onwude, Early detection of diseases in plant tissue using spectroscopy—applications and limitations. *Appl. Spectrosc. Rev.* **53**, 36–64 (2018).
  24. J. Lipiec, C. Doussan, A. Nosalewicz, K. Kondracka, Effect of drought and heat stresses on plant growth and yield: A review. *Int. Agrophys.* **27**, 463–477 (2013).
  25. A. Afzal, S. W. Duiker, J. E. Watson, Leaf thickness to predict plant water status. *Biosyst. Eng.* **156**, 148–156 (2017).
  26. T. Repo, Physical and physiological aspects of impedance measurements in plants. *Silva Fennica* **22**, 181–193 (1988).
  27. Y. Ando, S. Hagiwara, H. Nabetani, Thermal inactivation kinetics of pectin methylesterase and the impact of thermal treatment on the texture, electrical impedance characteristics and cell wall structure of Japanese radish (*Raphanus sativus* L.). *J. Food Eng.* **199**, 9–18 (2017).
  28. E. R. Hunt Jr., B. N. Rock, Detection of changes in leaf water content using near- and middle-infrared reflectances. *Remote Sens. Environ.* **30**, 43–54 (1989).
  29. Y. Shi, M. Manco, D. Moyal, G. Huppert, H. Araki, A. Banks, H. Joshi, R. McKenzie, A. Seewald, G. Griffin, E. Sen-Gupta, D. Wright, P. Bastien, F. Valceschini, S. Seité, J. A. Wright, R. Ghaffari, J. Rogers, G. Balooch, R. M. Pielak, Soft, stretchable, epidermal sensor with integrated electronics and photochemistry for measuring personal UV exposures. *PLOS ONE* **13**, e0190233 (2018).
  30. M. E. Lee, A. M. Armani, Flexible UV exposure sensor based on UV responsive polymer. *ACS Sens.* **1**, 1251–1255 (2016).
  31. M. I. N. Zhang, J. H. M. Willison, Electrical impedance analysis in plant tissues. *J. Exp. Bot.* **42**, 1465–1475 (1991).
  32. T. M. Murphy, Membranes as targets of ultraviolet radiation. *Physiol. Plant.* **58**, 381–388 (1983).
  33. J.-U. Sutter, U. Homann, G. Thiel, Ca<sup>2+</sup>-stimulated exocytosis in maize coleoptile cells. *Plant Cell* **12**, 1127–1136 (2000).
  34. J. H. Park, S. Choi, H. Moon, H. Seo, J. Kim, S.-P. Hong, B. S. Lee, E. Kang, J. Lee, D. H. Ryu, Antimicrobial spray nanocoating of supramolecular Fe (III)-tannic acid metal-organic coordination complex: Applications to shoe insoles and fruits. *Sci. Rep.* **7**, 6980 (2017).
  35. S. Kawashima, M. Nakatani, An algorithm for estimating chlorophyll content in leaves using a video camera. *Ann. Bot.* **81**, 49–54 (1998).
  36. C. Marionnet, C. Tricaud, F. Bernerd, Exposure to non-extreme solar UV daylight: Spectral characterization, effects on skin and photoprotection. *Int. J. Mol. Sci.* **16**, 68–90 (2014).
  37. J. F. Rubinson, Y. P. Kayinamura, Charge transport in conducting polymers: Insights from impedance spectroscopy. *Chem. Soc. Rev.* **38**, 3339–3347 (2009).
  38. P. Zoltowski, On the electrical capacitance of interfaces exhibiting constant phase element behaviour. *J. Electroanal. Chem.* **443**, 149–154 (1998).

**Acknowledgments:** We thank M. Formosi from the Durfee Conservatory at the University of Massachusetts Amherst for providing a wide variety of plant leaf and flower samples, S. Fan for drawing a plant cartoon, and H. J. Kim for invaluable discussions on bioimpedance spectroscopy. **Funding:** T.L.A. gratefully acknowledges financial support from the David and Lucile Packard Foundation for enabling the exploratory research reported here. **Author contributions:** J.J.K. and L.K.A. performed experiments, processed data, and helped write the manuscript. T.L.A. helped with data analysis and wrote and edited the manuscript. **Competing interests:** The authors declare that they have no competing interests. **Data and materials availability:** All data needed to evaluate the conclusions in the paper are present in the paper and/or the Supplementary Materials. Additional data related to this paper may be requested from the authors.

Submitted 13 November 2018  
 Accepted 29 January 2019  
 Published 15 March 2019  
 10.1126/sciadv.aaw0463

**Citation:** J. J. Kim, L. K. Allison, T. L. Andrew, Vapor-printed polymer electrodes for long-term, on-demand health monitoring. *Sci. Adv.* **5**, eaaw0463 (2019).

## Vapor-printed polymer electrodes for long-term, on-demand health monitoring

Jae Joon Kim, Linden K. Allison and Trisha L. Andrew

*Sci Adv* 5 (3), eaaw0463.  
DOI: 10.1126/sciadv.aaw0463

### ARTICLE TOOLS

<http://advances.sciencemag.org/content/5/3/eaaw0463>

### SUPPLEMENTARY MATERIALS

<http://advances.sciencemag.org/content/suppl/2019/03/11/5.3.eaaw0463.DC1>

### REFERENCES

This article cites 38 articles, 4 of which you can access for free  
<http://advances.sciencemag.org/content/5/3/eaaw0463#BIBL>

### PERMISSIONS

<http://www.sciencemag.org/help/reprints-and-permissions>

Use of this article is subject to the [Terms of Service](#)

---

*Science Advances* (ISSN 2375-2548) is published by the American Association for the Advancement of Science, 1200 New York Avenue NW, Washington, DC 20005. 2017 © The Authors, some rights reserved; exclusive licensee American Association for the Advancement of Science. No claim to original U.S. Government Works. The title *Science Advances* is a registered trademark of AAAS.